Journal of Photochemistry & Photobiology, A: Chemistry 457 (2024) 115879

Contents lists available at ScienceDirect

Journal of Photochemistry & Photobiology, A: Chemistry

journal homepage: www.elsevier.com/locate/jphotochem

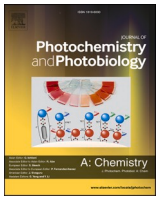

Identification of different WO_3 modifications in thin films for photocatalytic applications by peak shape analysis in high temperature XRD diffractometry

A. Brüger [a,*], G. Fafilek [a], M. Neumann-Spallart [b]

[a] Institute of Chemical Technologies and Analytics, Vienna University of Technology, Getreidemarkt 9/164, A-1060 Vienna, Austria
[b] Department of Inorganic Technology, University of Chemistry and Technology Prague, Technická 5, 16628 Praha 6, Czech Republic

ARTICLE INFO

Keywords:
WO_3
Photocatalysis
Phase Analysis
Thin Films

ABSTRACT

Until now, the structural analysis of WO_3 films has been insufficient. The similar peak positions of the possible crystalline phases make a precise differentiation difficult or even impossible. In particular, the presence of possible mixed phases is difficult to determine. However, the exact determination of the crystalline phases would be important for use as a photocatalyst, as these phases and also their mixtures may have an effect on the photocatalytic properties.

The identification of the monoclinic ($P2_1/n$), orthorhombic ($Pbcn$) and triclinic ($P\,\bar{1}$) components at room temperature seems to be of particular interest. By heating WO_3 films before cooling them to room temperature, a broadening of the diffraction peaks was observed, which can be associated with phase transformations. By following these peak broadenings, individual phases of WO_3 could be identified and the progression of mixed phases could be visualized. By avoiding a delamination process, which can occur at high temperatures, and an adapted heating strategy, it should be possible to identify different crystalline phases of WO_3 films at room temperature after calcination.

1. Introduction

The discrimination between different polymorphs of WO_3 is a crucial point in the evaluation of the properties of WO_3. Depending on the heating strategy, the compound is usually found as triclinic ($P\,\bar{1}$), monoclinic ($P2_1/n$, $P2_1/c$) orthorhombic ($Pbcn$) and tetragonal ($P4/nmm$, $P4/ncc$) [1 2] with the monoclinic $P2_1/n$ phase, most often found as the stable modification at room temperature. The exact determination of these phases is somehow difficult as the main reflections of the triclinic, the monoclinic $P2_1/n$ and the orthorhombic phase are found at similar positions. The discrimination in WO_3-powders can be done via high-resolution XRD or neutron powder diffraction analysis.

There are various applications of WO_3 like photocatalysis, electrochromic materials and gas sensing [3]. For gas sensing, the modification of WO_3 is of considerable importance as higher operation temperatures can be envisaged [4]. In photocatalysis carried out at room temperature, changes of properties after high temperature annealing followed by cooling may be expected due to structural and phase changes. The high temperature annealing used in the photocatalysis process is necessary for the crystallisation of the catalyst. WO_3 has the advantage over many comparable photocatalysts that it can be excited with visible light [5–7]. The use of WO_3 in photoelectrocatalysis involves depositing the catalyst on a conducting glass. This reduces the recombination of charge carriers [8–10]. When using conductive glass, however, heating is limited by the softening point of the glass used as a substrate and by the conductivity of the conductive layer [11]. In liquid phase applications, the coating of films on a substrate is preferred since the catalyst does not need to be separated from the solvent for reuse. Analysis of the crystallographic phases in films however is more difficult, as a coating changes the conditions for the formation of the catalyst particles compared to powders. Surface effects, particularly stress and strain, will have an influence on the film properties. The composition of precursor solutions for film deposition and post-annealing procedures leads to a wide range of factors that influence the particle composition in films, in particular the formation of different phases.

A close look at investigations on the crystallographic structure of WO_3 at RT reveals the existence of different modifications, depending on the preparation, the precursors and further treatment of the compound.

* Corresponding author.
E-mail address: brueger@tuwien.ac.at (A. Brüger).

https://doi.org/10.1016/j.jphotochem.2024.115879
Received 14 March 2024; Received in revised form 11 May 2024; Accepted 8 July 2024
Available online 9 July 2024

Table 1
Temperature ranges of different crystalline phases of WO_3 powders.

Crystal system	Space group	Temperature ranges (Howard, [1])
monoclinic	*Pc*	Below –23 °C (cited from [17])
triclinic	*P*1	−50 – RT °C (cited from [17])
monoclinic	$P2_1/n$	RT-350 °C
orthorhombic	*Pbcn*	350—720 °C
monoclinic	$P2_1/c$	720—800 °C
tetragonal	*P4/ncc*	800—900 °C
tetragonal	*P4/nmm*	900 °C and above

A pure triclinic phase or a mixture of the triclinic and monoclinic modification is found after cooling below RT or after a special heat treatment [12,13]. Low temperature monoclinic (*Pc*) WO_3 can be found besides these two phases at room temperature with mechanical stress conditions [14,15]. With a special pH and temperature strategy, orthorhombic WO_3 was synthesised at room temperature [5,6,16] while hexagonal tungsten trioxide was obtained with a hydrothermal method [9]. An overview of the temperature ranges of the different phases during heating of WO_3 powders according to Howard [1] is given in Table 1.

XRD-measurements for the identification of the different WO_3 phases are often combined with Rietveld refinement [1,5,18]. This method should make it possible to discriminate between two different overlapping peaks, necessary to differentiate between two phases with similar peak positions. However, the Rietveld method is defined for powders [19]. This does not mean that it cannot be used for films as well, but only using a large number of refinement parameters or degrees of freedom for the optimised fit of the curves, can allow the assessment of a particular phase. The literature does not provide quantification of the fractions of triclinic, monoclinic or orthorhombic modifications in a possible multi-phase powder of WO_3. Therefore, predicting the phase purity of films at room temperature using XRD analysis appears to be challenging. Another aspect complicates the peak refinement: the as grown films consist of small particles whose size may increase with deposition temperature. Depending on the heating strategy there will be a more or less strong peak broadening. For the identification of the peaks with the highest intensity, for triclinic, monoclinic and orthorhombic WO_3, these are the reflexes (0 0 2), (0 2 0) and (2 0 0), the positions are too close because the lattice spacings are very similar [18]. The typical splitting of lower intensity peaks is not clearly recognizable due to the peak broadening.

In addition to XRD analysis, Raman spectroscopy and TEM images can provide a deeper insight into the characterisation of tungsten trioxide films [20–22]. In Raman spectra, characteristic peaks for different WO_3 phases can be obtained. TEM images allow the identification of the different phases in measuring the lattice spacings. It appears that quantifying the WO_3 phase fractions in multi-phase films is not feasible.

Most of the photocatalytic studies of different modifications of WO_3 have been carried out with powders. Studies were found with orthorhombic WO_3 or a double phase including the monoclinic modification besides different multi phases including hexagonal, triclinic, orthorhombic and monoclinic modifications. Table 2 summarises publications cited in this work in preparation, described phases and photocatalysis. It should be noted that some of the publications listed do not describe an exact phase determination.

The investigation of photocatalytic properties using WO_3 layers presents challenges in structural elucidation compared to powders. This work examines two different layers to gain new insights into the WO_3 phase composition over a high range of temperatures. The study focuses on changes in peak shapes in XR diffractograms during phase transformations of the films.

Table 2
Catalyst Properties of samples investigated in some references in this publication.

Reference, Type of Catalyst, Initial Heating	Precursor	Described Phases, Phase Transformation Temperatures	Photocatalysis
[1] powder	reagent grade WO_3	See Table 1	no
[2] powder 1000 °C	ammonium paratungstate	monoclinic – orthorhombic: 293–352 °C orthorhombic – monoclinic P21/c coexistence: 714–759 °C tetragonal P4/ncc to P4/nmm heating: 845–925 °C Tetragonal P4/ncc to P4/nmm cooling: 875–910 °C	no
[5] powder 300–500 °C	sodium tungstate dihydrate and ammonium paratungstate	monoclinic-orthorhombic: 470 °C	MB-deg., argon-ion laser
[6] film 400 °C	tungsten foil, electrochemical anodization,	RT: orthorhombic	photo-current density, visible light illumination
[7] film 500 °C	tungsten foil, anodic oxidation	monoclinic	water splitting, xenon arc lamp
[8] film 450 °C	sodium tungstate dihydrate hydrothermal	monoclinic, hexagonal, depending on solvent	MB, rhodamine B, xenon arc lamp
[9] powder 400 °C	sodium tungstate dihydrate	RT: hexagonal/ triclinic mixture	MB-deg., hydrogen generation, xenon lamp
[12] powder 1200 °C	reagent grade WO_3	RT: mixture of monoclinic/triclinic RT after cooling to 0 °C: triclinic	no
[13] powder 700 °C	ammonium paratungstate	RT: mixture of monoclinic/triclinic	no
[14] powder >1000 °C	resistivity heating of W wires, application of an external electric field	RT: mixtures of monoclinic, triclinic, monoclinic-Pc depending on preparation	no
[15] powderRT	stoichiometric WO3 powder mild/ strong milling procedure, cooling to 40 K	RT: Mainly monoclinic or mainly triclinic or mixture with monoclinic-Pc, depending on temperature and milling	no
[16] powder 350 °C	WO_3 powder thermal vacuum evaporation	monoclinic/ orthorhombic (difficult to distinguish)	No
[18] powder	tungsten hexacarbonyl flame spray pyrolysis	orthorhombic-tetragonal (heating): ca 700 °C tetragonal-orthorhombic (cooling): 675 °C orthorhombic-monoclinic (cooling): 350–300 °C	no

(*continued on next page*)

Table 2 (*continued*)

Reference, Type of Catalyst, Initial Heating	Precursor	Described Phases, Phase Transformation Temperatures	Photocatalysis
[20] film 400 °C	tungsten foil, anodization	RT: predominantly orthorhombic	photo-current density, argon ion laser
[21] film	purchased WO_3 nanoparticles	monoclinic-orthorhombic (heating): 250 °C orthorhombic-tetragonal (heating): 750 °C tetragonal-orthorhombic (cooling): 700–800 °C orthorhombic-monoclinic (cooling) 200–150 °C	no
[22] powder	ammonium paratungstate freeze-drying/ spray pyrolysis	monoclinic-orthorhombic: 280 °C – 350 °C with larger particle size orthorhombic-tetragonal: 420—900 °C depending on particle size and pressure	no
[23] powder 400–500 °C	sodium tungstate dihydrate	triclinic, orthorhombic, monoclinic, depending on calcination temperature	MB – mercury lamp (365 nm)
[24] powder 500 °C	sodium tungstate dihydrate and ammonium tungstate hydrate	orthorhombic, close to monoclinic	rhodamine B mercury lamp (254 nm)
[25] film 350–650 °C	tungstic acid spray pyrolysis	monoclinic	photocurrent, xenon arc lamp

2. Materials and methods

Two types of films were prepared, one with an organic precursor (OP) and one with an inorganic precursor (IP). For the organic route, a round fused silica plate was spin coated with tungsten(V) ethoxide (Alfa Aesar) in isopropanol (0.4 M) (SÜSS MicroTec, 2000 rpm, 50 % rH). The coating was dried at 120 °C for 10 min, prior to the X-ray measurements. The inorganic route used peroxotungstic acid for the coating via aerosol pyrolysis with a deposition temperature of 400 °C [23]. The film thickness was 100 nm (OP) and 3.4 μm (IP).

Powder X-ray diffraction measurements were performed on a PANalytical X'Pert Pro diffractometer in Bragg-Brentano geometry using Cu Kα1,2 radiation filtered with a BBHD mirror and an X'Celerator linear detector. An Anton Paar HTK 1200 N high-temperature chamber was used for the *in-situ* monitoring of the experiments. The samples were heated from RT to 300 °C with a rate of 70 °C/min. the measurements beginning with 300 °C in 10 °C steps were performed with a heating rate of 5 °C/ min and a dwell time of 42 min. in the scan range of 2θ = 19 – 39 deg.

The diffractograms were evaluated using the PANalytical program suite HighScorePlus. A background correction by a method of Sonneveld and Visser was performed. Phase assignment was based on the ICDD-PDF5 + database 2024. Peak integration and area calculations were performed by profile fitting using this software. The observed diffractograms were background corrected and $K\alpha_2$ stripped for the presentation.

The SEM images were recorded on a Quanta 200 FEI (Thermo Fisher). The samples were covered by a thin metal layer before measurement.

3. Results and discussion

3.1. Structural characterization via XRD

The investigation of the WO_3 layers produced by the inorganic (IP) and organic (OP) routes was performed between 25 °C and 980 °C and after cooling down at 50 °C, (Fig. 1). The IP sample already shows crystalline structures at RT, as it was produced at 400 °C. The three reflections (0 2 2), (2 2 0) and (2 0 2) with their characteristic form can be assigned to the orthorhombic phase visible from around 450 °C. The intensities of two of the main reflections, (0 2 0) and (2 0 0), decrease at higher temperatures and the (1 1 0) reflection of the tetragonal phase becomes visible. The shift in most of the peaks to lower angles at higher temperatures can be explained by the increase of the cell dimensions with temperature. The phase identification of the two IP diffractograms in the RT range is rather difficult. With Rietveld-analysis the monoclinic phase would be favored to the triclinic and orthorhombic phase. However, this does not take into account the possible presence of mixed phases, as discussed in the introduction. A Rietveld-investigation of possible mixed phases triclinic/monoclinic/orthorhombic gave no meaningful results because the peak simulations were not comprehensible.

The OP sample shows a crystalline structure from just below 400 °C, as the film is amorphous after spin coating with organic residues that volatilize or decompose during the heating process, leading to incipient crystallisation at temperatures above 350 °C. The typical pattern of (0 2 2), (2 2 0) and (2 0 2) reflections of the orthorhombic phase seen with the IP probe is not visible. The crystallite growth in the (2 0 0) direction dominates the (0 2 0) and (0 0 2) directions. The progression of the transformation to the tetragonal phase is comparable to that of the IP sample.

In Fig. 1, reference patterns of monoclinic, orthorhombic and tetragonal WO_3 phases are added. Since the tetragonal reference was recorded at a temperature of 950 °C and the monoclinic pattern was made at RT, the two diffractograms were compared with the high-temperature results and the cooled sample, respectively. The orthorhombic, monoclinic ($P2_1/c$,) and tetragonal ($P4/ncc$), were correlated to the nearest OP sample temperature results. In order to obtain a more accurate comparison of the obtained diffractograms with the reference files, the measurements at the temperatures corresponding to the reference files were displayed in more detail.

In Fig. 2a and b the measurement of the as prepared IP sample and the diffractogram after the heat treatment together with the graph of the OP sample after cooling down are compared to a monoclinic $P2_1/n$ reference pattern. The pattern in Fig. 2c is compared with a tetragonal $P4/nmm$ reference file at 950 °C. Further correlations are given in Fig. 2d and e for orthorhombic and monoclinic $P2_1/c$ patterns. Although the diffractograms cannot be analyzed precisely with regard to their crystalline structure due to the fact that they were measured on layers with a small particle size, a relatively good agreement with the monoclinic ($P2_1/n$), orthorhombic and tetragonal ($P4/nmm$) reference files could be found. However, the differentiation of the phases at higher temperatures ($P2_1/c$, $P4/ncc$ and $P4/nmm$) was more difficult due to the closeness of the peaks in the measured range.

3.2. Investigation of phase transitions

3.2.1. Change of peak positions with temperature

Looking at the peak positions with increasing temperature in the 2θ range of 22.3 – 24.8 deg, the illustration in Fig. 3 shows a rather interesting progression of the peaks. The shift of the two outer peaks

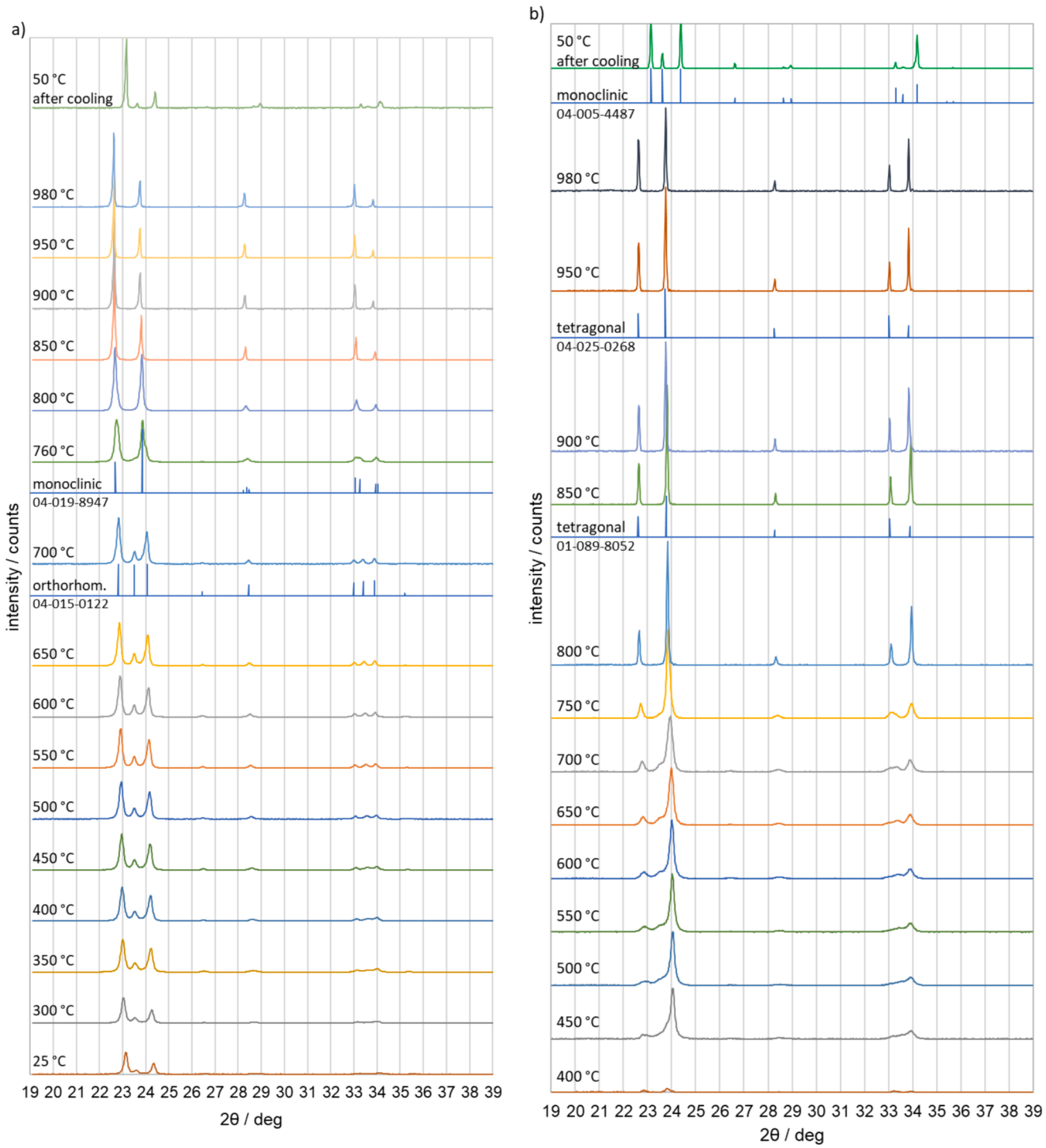

Fig. 1. X-ray diffractograms of IP (a) and OP (b) sample in 50 °C steps, and after cooling down to 50 °C reference patterns of an orthorhombic (Pbcn, 700 °C, [24] and a monoclinic ($P2_1/c$, 760 °C, [1]) phase below and above the diffractogram at 700 °C (a) and a monoclinic ($P2_1/n$, RT, [25]) and two tetragonal (P4/ncc, 827 °C [26] and P4/nmm, 950 °C, [1]) reference patterns below the diffractograms at 50 °C after cooling, 850 °C and 950 °C respectively (b).

seems linear at lower temperatures and shows variations in the high temperature range. The peak intensity is increasing in the low temperature range as expected due to the increase of crystallinity. At high temperatures the intensity is decreasing. The middle peak disappears with increasing temperature.

The left peak in Fig. 3 shows the (0 0 2) plane at lower temperatures and changes to the tetragonal (0 0 1) plane with heating. The right peak represents the (2 0 0) plane in the lower region changing to the tetragonal (1 1 0) plane at high temperatures. The middle peak is the (0 2 0) plane of the orthorhombic WO_3. It disappears with the phase transition.

A more detailed illustration of the evolution of the left and the right peak position of Fig. 3 is shown in Fig. 4. In comparing our data with the study of Howard [1] a similar progression of the peak shift in Fig. 3 to the lattice parameters a and c from neutron powder diffraction patterns can be observed. These similarities are an indication of a similar phase transformation taking place in our samples. The phase transition of orthorhombic WO_3 to the suggested $P2_1/c$ phase, indicated by the two curved parts from 720 °C (see also Fig. 5), is shown in Fig. 4 by the

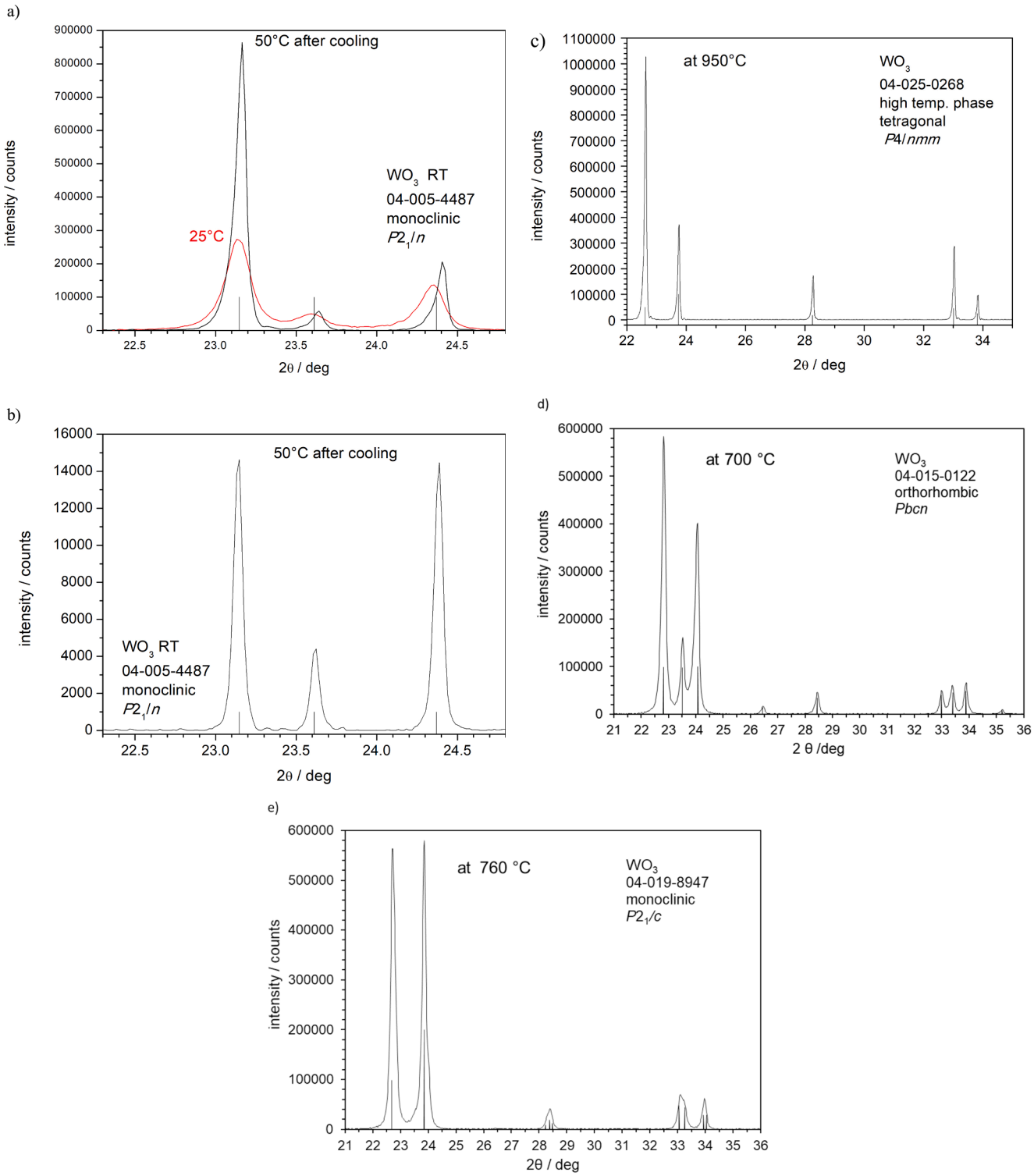

Fig. 2. Comparison of the diffractograms from measurements of the IP sample at 50 °C after cooling and 25 °C (red line) with a monoclinic reference pattern (a), the OP sample at 50 °C after cooling with the monoclinic pattern (b) and the IP sample measurement at 950 °C with a tetragonal *P4/nmm* (c), at 700 °C with an orthorhombic (d) and at 760 °C with a monoclinic $P2_1/c$ reference pattern (e) (see Fig. 1).

interrupted (002/001) curve. Two peak positions were determined from these changes in slope using peak refinement with profile fitting in the range between 720 °C and 760 °C, where this change of slope was clearly visible. The (200/110) curve is shown as a single line because no peak splitting was observed.

This seems not as pronounced in the OP sample. The shift of the position is slowed down before reaching 800 °C suggesting the transformation to the tetragonal *P4/ncc* phase and the further change at 890 °C to the tetragonal *P4/nmm* phase. The position of the orthorhombic plane (0 2 0) is not clearly shifted. It disappears at about 740 °C.

Obviously, it is not possible to make any precise statements about the crystalline state of our layers from this comparison. However, precise analysis of these films by XRD appears to be limited. Furthermore, the effect of heating the powders can only be compared to a limited extent

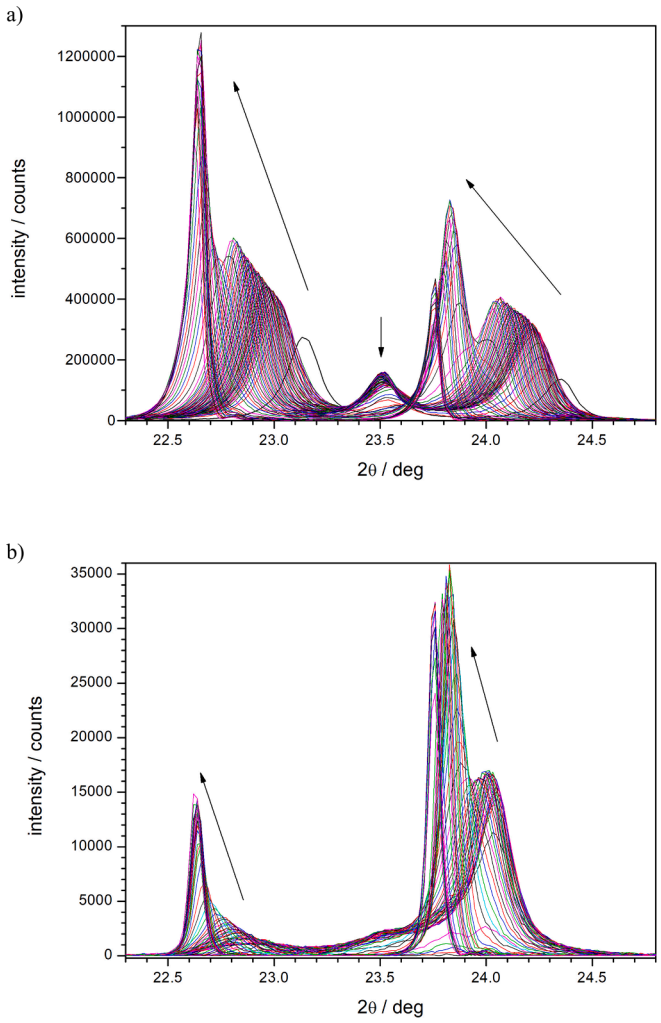

Fig. 3. Region between 2θ = 22.3 and 24.7 deg from the diffractograms over the entire temperature range, (a) IP sample, (b) OP sample (arrows show change in peak position with increasing temperature).

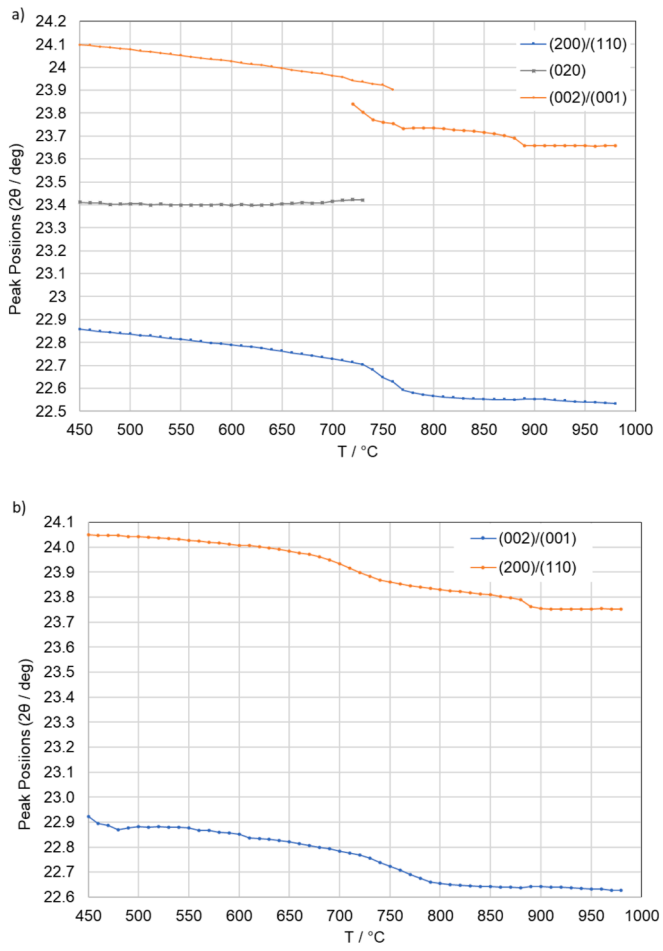

Fig. 4. Shift of the positions of three peaks, starting at low temperatures with the (002), (020) and (200) peak of the orthorhombic phase (a), IP sample, and the (002) and (200) peak (b) OP sample, respectively.

with the effects on the films, in particular the analysis of the occurrence of mixed phases is limited. Yet, it seems possible to draw conclusions from the neutron powder diffraction analyses about the evolution of the XRD measurements with respect to the structural change with increasing temperature [27].

For a more precise assessment of the phase transitions, a deeper analysis of the peaks is necessary.

3.2.2. *Transition of the orthorhombic phase at high temperature*

By plotting a smaller temperature range, the phase transformation from orthorhombic WO_3 to a possible monoclinic ($P2_1/c$) or tetragonal phase can be visualized (Fig. 5). The phase conversion in the IP sample is associated with a broadening of the left and right peak in the region between 2θ = 22.3 and 24.7 deg, resulting in the splitting of the right peak to a (1 1 0) and (2 0 0) part, most clearly shown at 740 °C. The right peak does not split due to the peak positions of the possible phases being too close. The transformation cannot be observed with this clarity in the OP sample but peak broadening is also evident and a shoulder at 720 °C indicates the transition of the orthorhombic phase.

It cannot be assumed that peak broadening is due to a reduction in crystallite size with increasing temperature. It is therefore reasonable to conclude that the formation of a second phase with similar peak positions leads to peak broadening, *i.e.*, a broadened peak actually consists of two peaks with similar positions which are not split. The broadening of the peaks is therefore analysed in more detail in the next section.

3.2.3. *Examination of peak broadening*

The peak broadening can be illustrated very well by determining the FWHM value at different temperatures (Fig. 6). It has to be pointed out that the FWHM in Fig. 6 does not represent the widths of single peaks. The growth of a second phase broadens the left peak of the IP sample, starting at 680 °C and the right peak starting at 720 °C. The bending of the curve of the left peak shortly after 800 °C and shortly before 900 °C can be seen as an indicator of the two further phase transformations. The broadening of both peaks around 300 °C suggests the transition from the monoclinic to the orthorhombic phase.

The peak broadening of the OP sample is more difficult to understand. Since the film was rather thin and the intensities of (2 0 0), (0 2 0) and (0 0 2) are very different, the change in the position of the (0 0 2) reflection in relation to the (0 2 0) peak seems to be the reason why the (0 0 2) peak appeared to broaden at lower temperatures (Fig. 5b). This is due to the different shifts of these two peaks with increasing the temperature and the lack of splitting. Only in the 700 °C range a significant peak broadening was detectable at the right peak, which can be attributed to the transition of the orthorhombic phase. All other marked changes in the linearity of the curve shown in Fig. 5a were most likely not found in the OP sample due to the small layer thickness.

3.3. *Area calculation by peak integration*

Information on crystallisation can be obtained by calculation of the

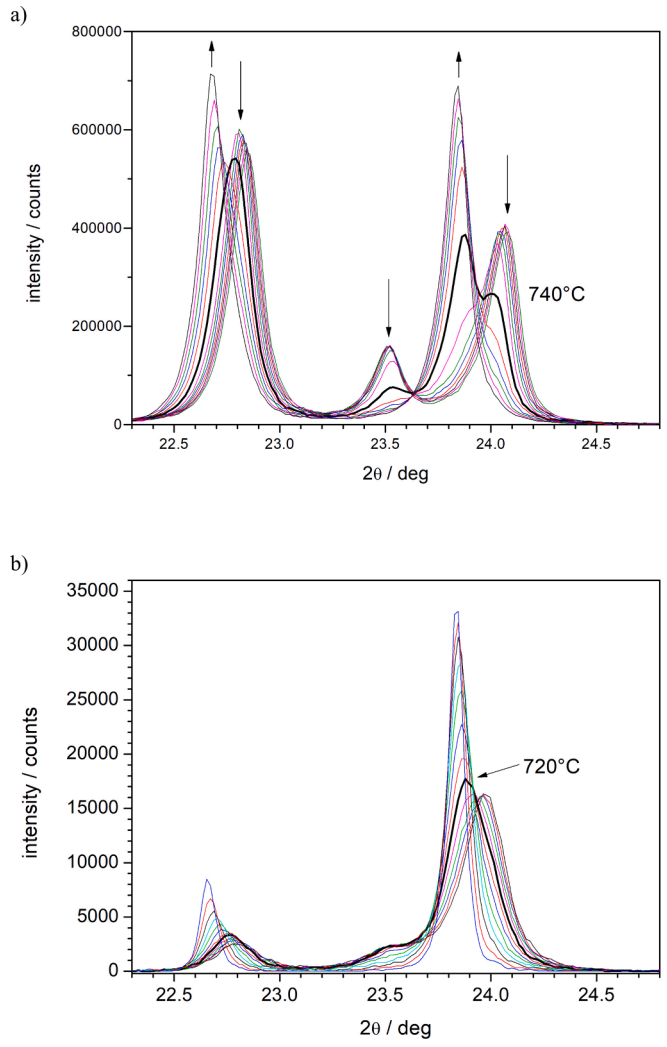

Fig. 5. Region between 2θ = 22.3 and 24.7 deg from the diffractograms in the range of 670 °C to 790 °C. (a) IP sample, (b) OP sample.

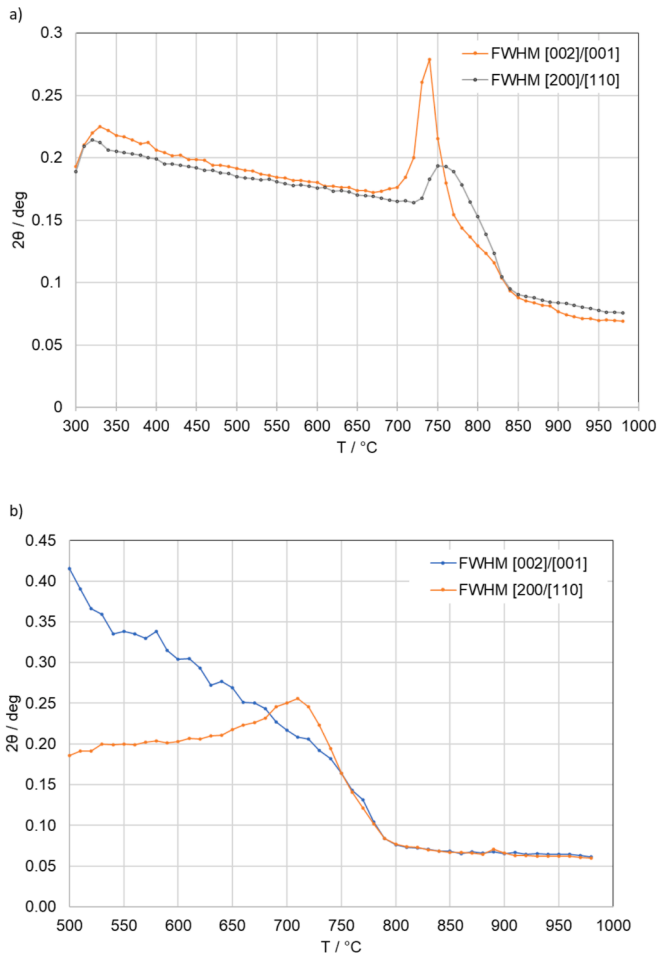

Fig. 6. Broadening of two diffraction peaks, starting at low temperatures with the (002) peak (left peak) and the (200) peak (right peak). (a) IP sample, (b) OP sample.

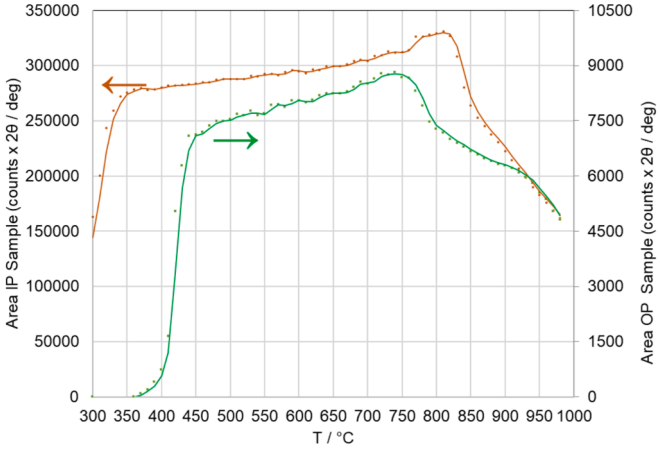

Fig. 7. Peak area calculation of the IP and OP sample over the entire temperature range.

area of the peaks from the X-ray measurement. In our diffractograms, the intensities over the whole investigated range were integrated. From this, the the extent to which the amorphous part of the layers decreased with the increase in temperature was estimated. Starting at 370 °C, a strong growth of the crystalline content in the OP sample is observed (Fig. 7). At around 450 °C a more or less even growth was visible up to 740 °C with an approx. 20 % increase in the peak area. Increasing the temperature, the peak area decreases. In studies on WO_3 powders at high temperatures sublimation was observed at temperatures far below the melting point [18]. In a former investigation by one of the authors, films produced with the same organic precursor disappeared at high temperatures. In using a cover glass resting on top of the film, the layers could be preserved with no residuals on the cover glass after cooling. As the decrease of the peak area was found in the same temperature range as the phase transformation, we assume that the film delaminated due to stress caused by the phase transitions and probably also due to the disappearance of by-products of condensation reactions to form WO_3, and decomposition products of the (organic) precursor (see also chapter 3.4).

The zone of even peak area increase was reached earlier with the IP sample as the layer already had a crystalline content at the beginning of the heating process. In the range between 350 and 750 °C, there was only a 13 % increase in the crystalline content, compared to the OP sample, then a stronger increase as the new phase became dominant, followed by a strong decrease. Delamination is visible at the edge of the sample after cooling. In both samples the crystalline content decreased to 47 % of the highest calculated area value. However, it must be assumed from the shape of the two curves of the area calculation that the crystallization of the originally amorphous layer or primarily amorphous layer in case of the IP sample was not complete at the beginning of delamination.

a)

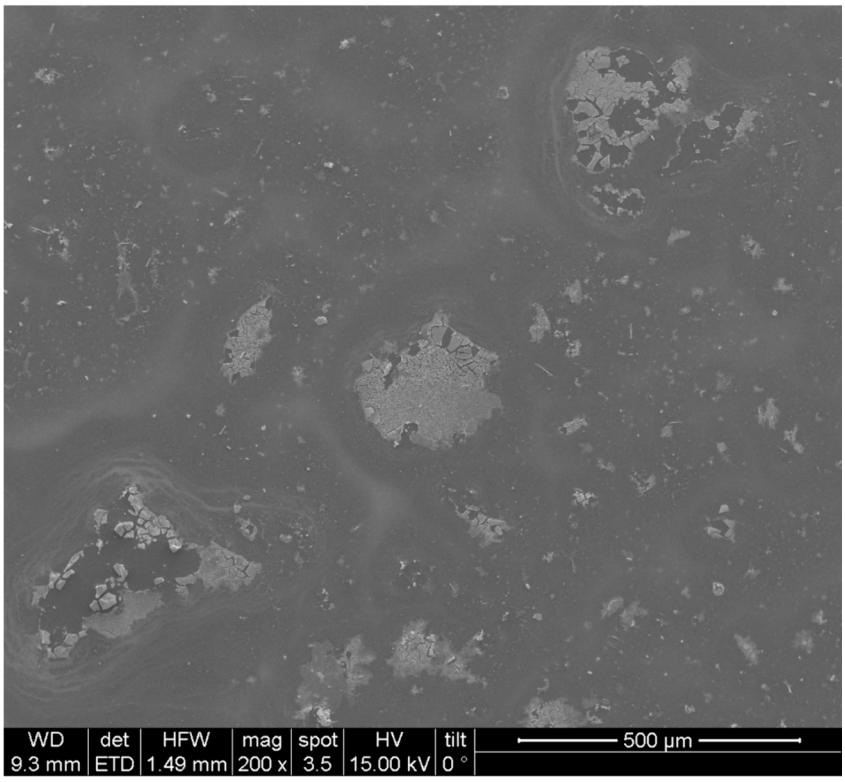

b)

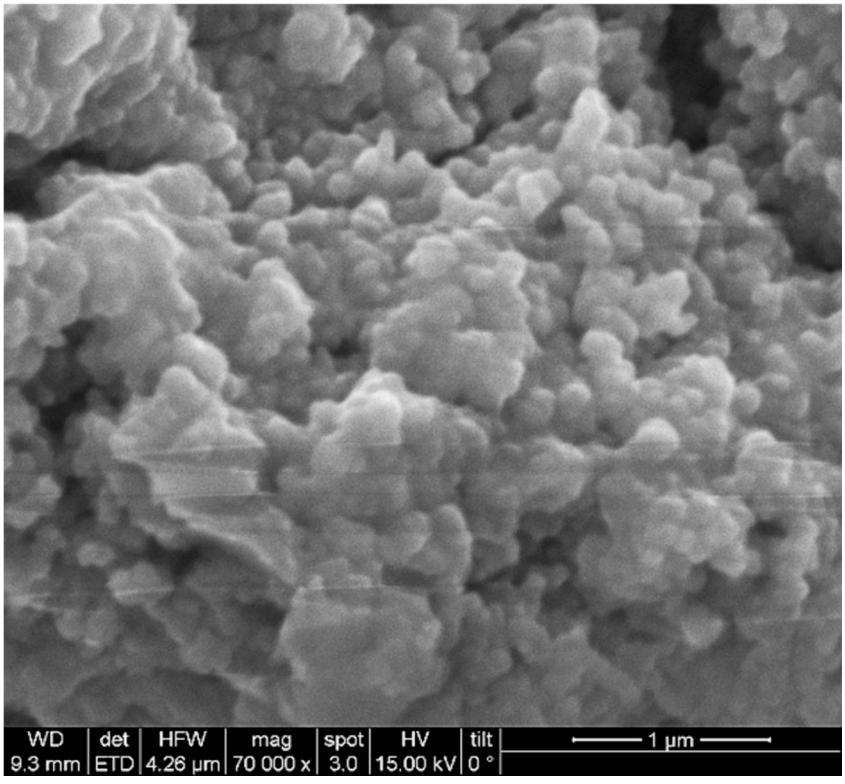

Fig. 8. SEM images of the OP sample with lower magnification (a) showing the delamination and high magnification (b) showing an undelaminated region of the film.

3.4. Scanning electron microscopy

The morphology of the OP sample was investigated by SEM imaging. The pictures of the film after the heat treatment confirm the loss of material (Fig. 8a). The film thickness of the as prepared layer was approx. 100 nm. After heating and cooling down, the crystallite size was estimated to be 130 – 200 nm using the Scherrer formula. In Fig. 8b, grains of approximately 200 nm are visible.

4. Conclusions

Phase identification of WO_3 is more difficult with films compared to powders. The different surface conditions, the influence of the substrate on the measurement and the production method have a major influence on the structural analysis. As a result, both the evolution of the phase transformations with temperature and the exact determination of the structure of WO_3 films at room temperature, in particular the presence of possible mixed phases, are difficult to assess.

By determining the structure of our films as a function of increasing temperature using small steps, peak changes and especially peak broadening became visible, which indicated phase transformations. These phase transformations were not really accessible by the direct evaluation of X-ray diffractograms for the reasons mentioned above. As the temperature of WO_3 films was increased, peak narrowing and crystallite growth would normally be expected. However, in the region of a phase transformation, no further peaks of a new phase were generally visible because the different phases of WO_3 that can be formed in the temperature range investigated here have very similar peak positions and therefore no peak splitting was visible, but peaks appeared broadened. The small crystallite size and the increased influence of the substrate at very thin layers with low intensities are other reasons why the peaks cannot be seen as separated, making it difficult to differentiate these effects.

The in-depth observation of the orthorhombic phase of WO_3 in the area of a peak broadening made it possible to visualise the separation of two peaks of different phases in a small temperature range. Subsequently, the non-linear progression of the peak narrowing at higher temperatures led to the conclusion that further phase transformations took place. Peak broadening was also observed in the phase transformation range between monoclinic $P2_1/n$ and orthorhombic WO_3.

This led to the conclusion that it is possible to visualize phase transformations in films, which are not normally visible in a diffractogram due to the lack of peak separation, by examining the peak change with temperature change in more detail. Furthermore, it should be possible to identify mixed phases at room temperature, as the crystallite is not expected to decrease upon cooling, which is why a peak broadening on cooling to room temperature should allow the identification and quantification of several phases.

Even if it were possible to produce WO_3 films with different pure phases, it would be a great challenge to determine the photocatalytic properties of the different phases, as these properties also depend on the morphology of the crystallinity and other factors. The main challenge would therefore be to be able to determine the influence of the different phases independently of the other influencing factors.

The disappearance of parts of the coating at high temperatures can be attributed to crystallite growth, stress in the films, disappearance of by-products of condensation reactions, and decomposition products (organic route), leading to cracking of the coating and breaking-up of fragments. In further experiments, we should be able to prevent delamination by avoiding the high temperature range and thus be able to analyse an undamaged WO_3 layer for possible mixed phases after cooling to room temperature. This could provide important information for use as a photocatalyst and, in particular, allow comparison of layers with different and defined phase structures.

Credit authorship contribution statement

A. Brüger: Writing – original draft, Visualization, Project administration, Methodology, Investigation, Data curation, Conceptualization. **G. Fafilek:** Writing – original draft, Visualization, Investigation, Conceptualization. **M. Neumann-Spallart:** Writing – original draft, Visualization, Investigation, Conceptualization.

Declaration of competing interest

The authors declare that they have no known competing financial interests or personal relationships that could have appeared to influence the work reported in this paper.

Data availability

Data will be made available on request.

Acknowledgements

The authors thank Werner Artner, Berthold Stöger, and Erich Halwax from the XRC - X-Ray Center of the TU-Vienna for the recording of the diffractograms and support with the evaluation, Elisabeth Eitenberger and Susanne Strobl (Institute of Chemical Technologies and Analytics – TU-Vienna) for the recording of the SEM-images and Martin Brada (UCT Prague, CZ) for the preparation of the IP film.

The authors acknowledge TU Wien Bibliothek for financial support through its Open Access Funding Program.

References

[1] C.J. Howard, V. Luca, K.S. Knight, High-temperature phase transitions in tungsten trioxide - the last word? J. Phys. Condens. Matter 14 (2002) 377–387, https://doi.org/10.1088/0953-8984/14/3/308.

[2] B. Han, A.V. Khoroshilov, A.V. Tyurin, A.E. Baranchikov, M.I. Razumov, O. S. Ivanova, K.S. Gavrichev, V.K. Ivanov, WO_3 thermodynamic properties at 80–1256 K revisited, J Therm Anal Calorim 142 (2020) 1533–1543, https://doi.org/10.1007/s10973-020-09345-z.

[3] S.S. Raj, N.S. G., S. S., Tungsten oxide-based materials: synthesis, properties, and applications, Nanomedicine & Nanotechnology Open Access 8 (2023) 000274. doi: 10.23880/nnoa-16000274.

[4] M. Modak, S. Rane, S. Jagtap, WO_3: a review of synthesis techniques, nanocomposite materials and their morphological effects for gas sensing application, Bull. Mater. Sci. 46 (2023) 28, https://doi.org/10.1007/s12034-022-02864-5.

[5] M. Desseigne, N. Dirany, V. Chevallier, M. Arab, Shape dependence of photosensitive properties of WO_3 oxide for photocatalysis under solar light irradiation, Appl. Surf. Sci. 483 (2019) 313–323, https://doi.org/10.1016/j.apsusc.2019.03.269.

[6] C. Ng, C. Ye, Y.H. Ng, R. Amal, Flower-Shaped Tungsten Oxide with Inorganic Fullerene-like Structure: Synthesis and Characterization, Cryst Growth Des 10 (2010) 3794–3801, https://doi.org/10.1021/cg100625m.

[7] M. Zych, K. Syrek, M. Pisarek, G.D. Sulka, Synthesis and characterization of anodic WO3 layers in situ doped with C, N during Anodization, Electrochim Acta 411 (2022) 140061, https://doi.org/10.1016/j.electacta.2022.140061.

[8] L. Li, J. Li, H. BoK, J.H. Kim, The effect of morphology and crystal structure on the photocatalytic and photoelectrochemical performances of WO3, RSC Adv 14 (2024) 2080–2087, https://doi.org/10.1039/D3RA07329G.

[9] K. Ito, R. Uchida, K. Noda, Visible light-assisted hydrogen generation over platinum-loaded tungsten trioxide nanorods with the hexagonal and triclinic phases, J Photochem Photobiol A Chem 443 (2023) 114824, https://doi.org/10.1016/j.jphotochem.2023.114824.

[10] A. Brüger, G. Fafilek, M. Neumann-Spallart, Treatment of cyanide: Photoelectrocatalytic degradation using TiO_2 thin film electrodes and influence of volatilization, Sol. Energy 205 (2020) 74–78, https://doi.org/10.1016/j.solener.2020.05.035.

[11] T. Imrich, H. Krýsová, M. Neumann-Spallart, J. Krýsa, Pseudobrookite (Fe_2TiO_5) films: Synthesis, properties and photoelectrochemical characterization, Catal Today 413–415 (2023) 113982, https://doi.org/10.1016/j.cattod.2022.12.013.

[12] P.M. Woodward, A.W. Sleight, T. Vogt, Structure refinement of triclinic tungsten trioxide, J. Phys. Chem. Solid 56 (1995) 1305, https://doi.org/10.1016/0022-3697(95)00063-1.

[13] A.G. Souza Filho, J. Mendes Filho, V.N. Freire, A.P. Ayala, J.M. Sasaki, P.T. C. Freire, F.E.A. Melo, J.F. Juliao, U.U. Gomes, Phase transition in WO_3 microcrystals obtained by sintering process, J. Raman Spectrosc. 32 (2001) 695–699.

[14] B. Rodriguez, J. Dolado, J. Lopez-Sanchez, P. Hidalgo, B. Mendez, Room Temperature Polymorphism in WO_3 Produced by Resistive Heating of W Wires, Nanomaterials 13 (2023) 884, https://doi.org/10.3390/nano13050884.
[15] E. Cazzanelli, C. Vinegoni, G. Mariotto, A. Kuzmin, J. Purans, Low-Temperature Polymorphism in Tungsten Trioxide Powders and Its Dependence on Mechanical Treatments, J Solid State Chem 143 (1999) 24–32, https://doi.org/10.1006/jssc.1998.8061.
[16] M.F. Al-Kuhaili, T.F. Qahtan, M.B. Mekki, Temperature-dependent electrical resistivity of tungsten oxide thin films, J. Phys. Chem. Solid 182 (2023) 111607, https://doi.org/10.1016/j.jpcs.2023.111607.
[17] E.K.H. Salje, S. Rehmann, F. Pobell, D. Morris, K.S. Knight, T. Herrmannsdorfer, M. T. Dove, Crystal structure and paramagnetic behavior of ε-WO_3-x, J. Phys. Condens. Matter 9 (1997) 6563–6577, https://doi.org/10.1088/0953-8984/9/31/010.
[18] S. Pokhrel, J. Birkenstock, A. Dianat, J. Zimmermann, M. Schowalter, A. Rosenauer, L.C. Ciacchi, L. Maedler, In situ high temperature X-ray diffraction, transmission electron microscopy and theoretical modeling for the formation of WO_3 crystallites, CrstEngComm 17 (2015) 6985–6998, https://doi.org/10.1039/c5ce00526d.
[19] H.M. Rietveld, The Rietveld method, A Retrospection, Zeitschrift Fuer Kristallographie - Crystalline Materials 225 (2010) 545–547, https://doi.org/10.1524/zkri.2010.1356.
[20] A.Z. Sadek, H. Zheng, M. Breedon, V. Bansal, S.K. Bhargava, K. Latham, J. Zhu, L. Yu, Z. Hu, P.G. Spizzirri, W. Wlodarski, K. Kalantar-Zadeh, High-Temperature Anodized WO_3 Nanoplatelet Films for Photosensitive Devices, Langmuir 25 (2009) 9545–9551, https://doi.org/10.1021/la901944x.
[21] K. Thummavichai, N. Wang, F. Xu, G. Rance, Y. Xia, Y. Zhu, In situ investigations of the phase change behavior of tungsten oxide nanostructures, R Soc Open Sci 5 (2018) 171932/1, https://doi.org/10.1098/rsos.171932.
[22] M. Boulova, G. Lucazeau, Crystallite Nanosize Effect on the Structural Transitions of WO_3 Studied by Raman Spectroscopy, J Solid State Chem 167 (2002) 425–434, https://doi.org/10.1006/jssc.2002.9649.
[23] M. Brada, M. Neumann-Spallart, J. Krysa, Tungsten trioxide film photoanodes prepared by aerosol pyrolysis for photoelectrochemical applications, Catal Today 413–415 (2023) 113981, https://doi.org/10.1016/j.cattod.2022.12.012.
[24] T. Vogt, P.M. Woodward, B.A. Hunter, The High-Temperature Phases of WO_3, J Solid State Chem 144 (1999) 209–215, https://doi.org/10.1006/jssc.1999.8173.
[25] S. Tanisaki, Crystal structure of monoclinic tungsten trioxide at room temperature, J Physical Soc Japan 15 (1960) 573, https://doi.org/10.1143/jpsj.15.573.
[26] K.R. Locherer, I.P. Swainson, E.K.H. Salje, Transition to a new tetragonal phase of WO_3: crystal structure and distortion parameters, J. Phys. Condens. Matter 11 (1999) 4143–4156, https://doi.org/10.1088/0953-8984/11/21/303.
[27] K.R. Locherer, E.K.H. Salje, The refinement of a tetragonal phase of WO_3 using a novel PSD high temperature x-ray powder diffractometer, Phase Transit. 69 (1999) 85–93, https://doi.org/10.1080/01411599908208010.